Materials Today Bio 21 (2023) 100697

Contents lists available at ScienceDirect

Materials Today Bio

journal homepage: www.journals.elsevier.com/materials-today-bio

A targeted activatable NIR-II nanoprobe for positive visualization of anastomotic thrombosis and sensitive identification of fresh fibrinolytic thrombus

Ying Yuan [a,1], Shanchao Diao [b,1], Dong Zhang [a], Wanrong Yi [a], Baiwen Qi [a], Xiang Hu [a], Chen Xie [b,***], Quli Fan [b,**], Aixi Yu [a,*]

[a] Department of Orthopedics Trauma and Microsurgery, Zhongnan Hospital of Wuhan University, Wuhan, 430071, China
[b] State Key Laboratory of Organic Electronics and Information Displays, and Jiangsu National Synergetic Innovation Center for Advanced Materials (SICAM), Institute of Advanced Materials (IAM), Nanjing University of Posts & Telecommunications, Nanjing, 210023, China

ARTICLE INFO

Keywords:
Protein disulfide isomerase
Activatable probe
Thrombosis
Fibrinolytic thrombus
Supramolecular complex
NIR-II

ABSTRACT

Anastomotic thrombosis prevalently causes anastomosis failure, accompanied with ischemia and necrosis, the early diagnosis of which is restricted by inherent shortcomings of traditional imaging techniques in clinic and lack of appropriate prodromal biomarkers for thrombosis initiation. Herein, a fresh thrombus-specific molecular event, protein disulfide isomerase (PDI) is innovatively chosen as the activating factor, and a thrombosis targeting and PDI-responsive turn-on near infrared II (NIR-II) fluorescence nanoprobe is firstly developed. The supramolecular complex-based nanoprobe IR806-PDA@BSA-CREKA is fabricated by assembling NIR-II emitting cyanine derivative IR806-PDA with bovine serum albumin (BSA), which could ameliorate the stability and pharmacokinetics of the nanoprobe, addressing the contradiction in the balance of brightness and biocompatibility. The NIR–II–off nanoprobe exhibits robust turn-on NIR-II fluorescence upon PDI-specific activation, *in vitro* and *in vivo*. Of note, the constructed nanoprobe demonstrates superior photophysical stability, efficient fibrin targeting peptide-derived thrombosis binding and a maximum signal-to-background ratio (SBR) of 9.30 for anastomotic thrombosis in NIR-II fluorescent imaging. In conclusion, the exploited strategy enables positive visualized diagnosis for anastomotic thrombosis and dynamic monitoring for thrombolysis of fresh fibrinolytic thrombus, potentially contributes a novel strategy for guiding the therapeutic selection between thrombolysis and thrombectomy for thrombosis treatment in clinic.

1. Introduction

In clinic, vascular anastomotic surgeries are generally performed in cases that vascular injury/vascular ruptures exist, or that flap transplantation/organ transplantation is needed. Among these, 5% of free tissue transplantation, 10–30% of replantation of severed limbs cannot survive, and a considerable proportion of organ transplantation fails [1], as a result of anastomotic thrombosis, thromboembolism, or rejection-derived thrombosis, which can cause necrosis of tissues and organs, and even life-threatening renal failures [2]. Nowadays, the diagnostic sensitivity and accuracy of anastomotic thrombosis are restricted by the lack of efficient detection for the prodromal biomarkers of thrombosis and the fact that mainstream imaging methods are based on negative imaging (namely "signal defect"). Moreover, the dynamic monitoring of thrombolysis is still challenging, due to the insufficient imaging efficiency and convenience [2], and being unable to distinguish the change in thrombotic compositions, which can markedly affect the thrombolytic efficacy and safety [3]. Therefore, revolted imaging

Abbreviations: PDI, protein disulfide isomerase; SBR, signal-to-background ratio; BSA, bovine serum albumin; rt-PA, recombinant tissue plasminogen activator; TEM, transmission electron microscopy; DLS, dynamic light scattering; FITC, fluorescein isothiocyanate.

* Corresponding author.
** Corresponding author.
*** Corresponding author.
E-mail addresses: iamcxie@njupt.edu.cn (C. Xie), iamqlfan@njupt.edu.cn (Q. Fan), yuaixi@whu.edu.cn (A. Yu).
[1] These authors contributed equally to this work.

https://doi.org/10.1016/j.mtbio.2023.100697
Received 25 April 2023; Received in revised form 29 May 2023; Accepted 7 June 2023
Available online 9 June 2023

techniques and molecular probes that can reflect the occurrence of molecular events by imaging signal changes are urgently needed to be exploited, for the diagnosis of anastomotic thrombosis and the monitoring of thrombolytic therapies.

As a revolutionary strategy, imaging probes have evolved from "always on" contrast agents to activatable probes which can change their signals in response to stimuli derived from pathophysiology-specific molecular alterations, including enzymes, pH, redox environment [4–6], providing a higher signal-to-background ratio (SBR) with concentration-independent signal activation and contributing to a better sensitivity and specificity, and lower detection limits [7]. To realize the goal of early diagnosis of thrombosis and dynamic monitoring of thrombolysis, an appropriate bio-stimulus is to be explored. Among the thrombosis related molecular events, a new one namely protein disulfide isomerase (PDI) which plays a vital role in regulating the activation and formation of the three major components in thrombosis (platelets, coagulation factors, fibrin) has been characterized as a therapeutic target in antithrombotic therapies [8,9]. At the beginning of thrombosis, PDI in oxidation state shift into enzymatically active reduced form upon platelet activation [10], which not only accelerates the platelet aggregation [11], but also initiates the formation of fibrin [12]. The fact that PDI enzymatic reductive activity only exists on the surface of activated platelet in fresh thrombus [13] permits it a key bio-stimulus for activatable probes to identify fresh thrombosis. Currently, no activatable probes have been designed to response to PDI enzymatic activity. In this study, a PDI-activatable probe was designed for positive visualization of fresh thrombosis, aiming to improve imaging sensitivity and accuracy, and to distinguish fresh thrombus from old ones.

The appropriate selection of prodromal biomarkers of thrombosis initiation is particularly critical to improve the selectivity and specificity of probes for early diagnosis. In the past years, RGD, a targeted peptide to ligand activated platelets, has been universally used to target thrombosis [14]. As a matter of fact, the activated and aggregated platelets do not necessarily see a formation of thrombus, they can still be dispersed by the blood flow instead. In contrast, fibrin, which can cross-link to constitute dense fibrin network which protects the blood clot from collapse by mechanical stress and proteolysis, is considered as the initial molecular event of irreversible blood clot formation in the process of thrombosis [15], and can be chose as the exact prodromal biomarker of thrombosis initiation. In addition, fibrin itself, is the fibrinolytic substrate of recombinant tissue plasminogen activator (rt-PA), the most important choice for thrombosis-related disease treatments [16]. Afterwards, fibrin will constantly degrade to non-fibrinolytic collagen and elastic fibers with the evolution of thrombotic compositions, predicting a decrease of thrombolysis efficiency [17,18]. Therefore, fibrin is a well-deserved biomarker for identification of the thrombosis initiation as well as distinguishing thrombus those can be efficiently fibrinolytic. Thus, a fibrin targeting peptide CREKA (Cys-Arg-Glu-Lys-Ala) was selected to provide with targeted binding to thrombosis.

In the past decades, fluorescence imaging technique in the second near-infrared window (NIR-II, 1000–1700 nm) has gain extensive attention in biological theranostic applications [19–22]. However, further clinical transformation is decelerated by the contradiction in the balance of brightness and biocompatibility of the fluorophores. Among the reported fluorophores, cyanine dyes with a large π-conjugated system can maintain their excellent brightness *in vivo* due to their high molar extinction coefficient and moderate fluorescence quantum yields (QYs) [23–25]. However, a wider clinical application has been restricted by the impaired stability of cyanine dyes under NIR fluorescence excitation [26,27]. Serum albumins, with high biocompatibility and hydrophobic pockets in which small molecular dyes can be encapsulated, have been investigated to construct cyanine@albumin supramolecular complexes for the better stability, enhanced fluorescence emission and higher QYs [28–30]. Supramolecular complexes assembled based on albumin has been proved to provide a protein scaffold to stabilize the relativity flexible fluorophores to reduce the nonradiation processes, to improve the QYs and lifetime of fluorophores, and even to enhance therapeutic effects [28,31]. Here, we hypothesized the synthesized cyanine derivative can be assembled into BSA, to prepare a nanoprobe with better stability, longer emission and better imaging efficiency.

Herein, on the basis of our previous work [14,32,33] and existing research progress, we developed a novel supramolecular complex-based fibrin-targeted and PDI-responsive NIR-II probe (IR806-PDA@BSA--CREKA). As shown in Scheme 1, IR806-PDA@BSA-CREKA mainly includes 3 components: 1) cyanine derivative IR806-pyridine dithioethylamine (IR806-PDA), the disulfide bond of IR806-PDA can be isomerized under the catalysis of PDI, the obtained catalysate exhibits NIR-II fluorescence; 2) bovine serum albumin (BSA) and IR806-PDA are assembled into supramolecular complex, which largely enhances the stability and further redshifts the emission peak; 3) CREKA peptide (Cys-Arg-Glu-Lys-Ala), is used to specifically target fibrin. Driven by targeted peptide, IR806-PDA@BSA-CREKA is linked to thrombus, thus it can response to the PDI on the surface of activated platelets and emerged with NIR-II fluorescence, so as to realize rapid and sensitive early diagnosis of thrombosis, and thrombolysis monitoring of fibrinolytic thrombus, and to provide technical support for the accurate visualized diagnosis and the guide for thrombosis treatment selection.

2. Materials and methods

2.1. Materials

IR806, BSA, PDI (P3818), DTT (D0632), PDI inhibitor 16F16 (SML0021) were purchased from Sigma-Aldrich. Pentapeptide CREKA were customized from GL biochem (shanghai) Ltd. Rt-PA (Actilyse®/Alteplase) was obtained from Zhongda Hospital of Wuhan University. The recombinant Anti-Fibrinogen alpha chain (ab92572; 1:400 diluted) was purchased from Abcam, and Cy™3 AffiniPure Donkey Anti-Rabbit IgG (H + L) (711-165-152; 1:400 diluted) was purchased from Jackson ImmunoResearch. All other standard reagents were purchased from commercial suppliers (such as Ponsure Biological) and used without further purification. NIH3T3 (mouse fibroblast cell line) cells, and RAW264.7 (mouse macrophages cell line) cells were obtained from Key Gene Tech Co. (Shanghai, China), cultured in Dulbecco's Modified Eagle's Medium (DMEM, Gibco, U.S.), supplemented with 10% FBS (Gibco, Grand Island, NY, USA), at 37 °C in a humidified incubator containing 5% CO_2.

2.2. Synthesis of IR806-PDA

According to the previous synthesis method [32], IR806 (100 mg, 0.136 mmol) and 2 - (pyridin-2-yldisulfide) ethyl-1-amine hydrochloride (33.3 mg, 0.15 mmol) were mixed in argon atmosphere. Then, the mixture was added with TEA (0.5 mL) and N, *N*-dimethylformamide (DMF) (20 mL) and stirred at room temperature until the solution completely turned blue. Then the mixture was poured into ether for precipitation, and purified by column chromatography (silica gel, methanol/dichloromethane = 1/10) to obtain 75.6 mg (62.9%) of blue solid IR806-PDA (Fig. S1A). ^{1}H NMR (400 MHz, Methanol-d4, ppm) δ: 8.44–8.36 (s, 1H), 7.94–7.86 (d, J = 12.6 Hz, 2H), 7.82–7.69 (d, J = 3.7 Hz, 3H), 7.43–7.27 (m, 6H), 7.17–7.06 (m, 4H), 4.19–4.12 (s, 2H), 4.06–3.95 (s, 4H), 2.96–2.89 (s, 4H), 2.84–2.74 (s, 4H), 2.24–1.85 (s, 14H), 1.75–1.58 (s, 12H). MALDI-TOF MS (m/z): 862.992 $[M\text{-}Na+2H]^+$.

2.3. Construction of IR806-PDA@BSA

BSA was dissolved in 1 × PBS (pH = 7.4), the concentration is adjusted to 20 mg mL^{-1}. IR806-PDA was dissolved in dimethyl sulfoxide (DMSO) at a concentration of 26.7 mM. Glutathione (GSH) was dissolved in 10% DMSO/PBS buffer solution with a concentration of 0.25 M.

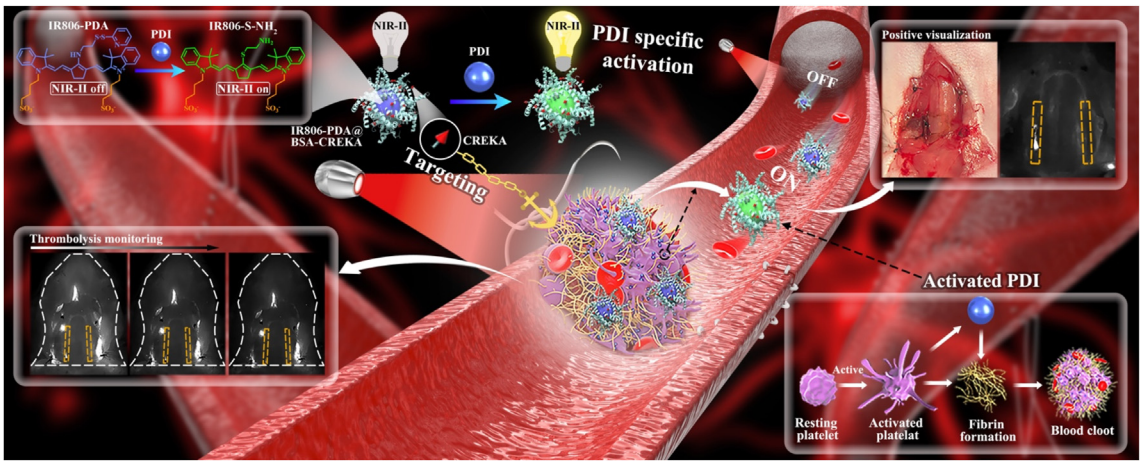

Scheme 1. Schematic illustration for IR806-PDA@BSA-CREKA nanoprobe activation and targeting, and IR806-PDA@BSA-CREKA-mediated specific positive visualization and thrombolysis monitoring of anastomosis thrombosis.

Glutaric dialdehyde (GTD) was dissolved in PBS with a concentration of 0.25 M. The BSA solution (1 mL, 20 mg mL^{-1}) was pretreated with 60 μL GSH solution (0.25 M), and stirred at room temperature for 12 h. The solution was washed 3–4 times with PBS and filtrated with 30 kDa ultrafiltration centrifugal filter to remove excess GSH. Then, the pretreated BSA solution (1 mL) and the IR806-PDA solution (26.7 mM, 11 μL) were mixed and shaken at 37 °C for 24 h. Subsequently, the GTD (24 μL 0.25 M) solution was added into the mixture and heated at 60 °C for 10 min. The reactive product was centrifuged (30 kDa ultrafiltration centrifugal filter) and washed to obtain IR806-PDA@BSA.

2.4. Preparation of nanoprobe IR806-PDA@BSA-CREKA

The pentapeptide CREKA (2 mg) was firstly reacted with sulfo-SMCC (2 mg) in PBS (1 mL) at 37 °C for 2 h, and added with IR806-PDA@BSA for following 24 h. The reactive product was washed and centrifuged (30 kDa ultrafiltration centrifugal filter) to get IR806-PDA@BSA-CREKA (Fig. S1B).

2.5. Instruments and general experimental methods

The ^{1}H NMR spectra were performed on a Bruker Ultra Shield Plus 400 MHz spectrometer. MALDITOF-MS characterizations were performed on an Ultraflextreme MALDI-TOF mass spectrometer (Bruker Daltonics Inc., Nasdaq, USA), and α-Cyano-4-hydroxyc innamicacid (HCCA) was selected as matrix. The morphology of nanoparticles was observed by transmission electron microscopy (TEM) (Hitachi HT7700) with an acceleration voltage of 100 KV. Dynamic light scattering (DLS) analyses were conducted on a commercial laser light scattering spectrometer (ALV-7004; ALVGmbH, Langen, Germany) equipped with a multi-τ digital time correlator and a He–Ne laser (λ = 632.8 nm). All samples we used for the test were optically cleared by filtration via 0.45 μm Millipore filter. The scattering angle was set up to 90° and all tests were conducted under room temperature. A UV–vis spectrophotometer (Nanjing Feile Instrument Co., Ltd.) was utilized to record the absorption spectra of the samples at room temperature. Fluorescence spectra were recorded on a NIR-II spectrophotometer (Fluorolog 3, Horiba). NIR-II FI experiments of cells and animals were conducted on an NIR-II fluorescence imaging system (Wuhan Grand-imaging Technology Co., Ltd) with 980 nm filter under the 808 nm laser irradiation. The NIR-II FI system were equipped with a 640 × 512 pixels two-dimensional InGaAs array from Princeton Instruments in NIR-II fluorescence windows. The MTT analyses were carried out on a Power Wave XS/XS2 microplate spectrophotometer (BioTek, Winooski, VT).

2.6. Theoretical calculation

All the calculations were performed with the Gaussian 16 program [34]. The geometric optimization of the complexes was performed at B3LYP/6-31G(d) level by means of the density functional theory method [35]. The drawing of molecular orbital diagrams was carried out by the Multiwfn_3.8_dev program [36].

2.7. Photophysical properties

2.7.1. Stability

The stability of diameters was detected by DLS as aforementioned, using IR806-PDA@BSA-CREKA dissolved in 1 × PBS (pH = 7.4), and 10% FBS solutions at different time points (0 d, 1 d, 5 d, 7 d). The absorption stability of IR806-PDA, IR806-PDA@BSA, IR806-PDA@BSA-CREKA aqueous solution was recorded using UV–vis spectrophotometer (1 d, 2 d, 3 d, 4 d, 6 d), from 500 nm to 900 nm.

2.7.2. Photostability

Photobleaching study was performed to compare the photostability of IR806-PDA@BSA-CREKA with the commercial cyanine ICG. ICG and IR806-PDA@BSA-CREKA (20 μg mL^{-1}) were respectively irradiated by 635 nm laser (1 W cm^{-2}). The absorption was evaluated at different time post irradiation (0 min , 5 min , 10 min , 15 min , 20 min , 25 min , 30 min).

2.8. SDS-PAGE assay

Prepare concentrated glue and separating glue according to the instructions. All samples: marker (3 μL), IR806-PDA (30 μg mL^{-1}, 10 μL), BSA (5 mg mL^{-1}, 3 μL), IR806-PDA@BSA (30 μg mL^{-1}, 10 μL), IR806-PDA@BSA-CREKA (30 μg mL^{-1}, 10 μL) were loaded into the gel holes accompanied with protein buffer solution (volume ratio 4:1) and were electrophoresed at 110 V on the vertical electrophoresis system. Finally, the PAGE gel was visualized using the IVIS *in vivo* imaging system, with the excitation wavelength of 670 nm and the emission wavelength of 740 nm.

2.9. In vitro studies

2.9.1. Cytotoxicity assessment

NIH3T3 and RAW264.7 cells were cultured in 96-cell plates at a density of 8000 cells per well overnight. Then the cells were incubated with 100 μL of fresh cell meadia containing 0, 5, 10, 20, 30, 40, 50, 60 μg mL^{-1} of nanoprobe for 24 h. Then MTT (0.5 mg mL^{-1}) was added into

each well (20 μL) and incubated at 37 °C for 4 h. Dimethyl sulfoxide (DMSO) (100 μL) was added to resolubilize the formazan. The absorbance at 490 nm was measured with a Bio-Tek Synergy HTX. The cell viability was calculated in accordance with the following formula: Cell viability (%) = (mean of absorbance value of treatment group/mean of absorbance value of control) × 100.

2.9.2. PDI activation in vitro

IR806-PDA@BSA-CREKA was determined at a final concentration of 10 μg mL^{-1}, and incubated with different concentrations of PDI solution (0.1, 0.2, 0.4, 0.6, 0.8 μM) for 1 h. PDI was add with corresponding concentrations of DTT (0.1, 0.2, 0.4, 0.6, 0.8 mM) for 10 min, before the incubation. The changes of absorbance, fluorescent intensity, NIR-II fluorescence signal of the nanoprobe incubated with different concentrations of PDI for different time were respectively recorded by UV–vis spectrophotometer, NIR-II spectrophotometer (external 808 nm laser, 1 W cm^{-2}), NIR-II fluorescence imaging system (808 mm laser, 40 mW cm^{-2}, 980 nm filter, 30 ms exposure), and fitted to a linear curve.

2.9.3. In vitro blood clot targeting assessment

(1) Establishment of blood clot

The whole blood of mice was used to prepare fresh blood clots. The whole blood of mice was collected with EP tube without anticoagulant, transfer it to 96 well plate immediately after the collection, 200 μL per well. Then, the 96 well plate was placed at 4 °C overnight to form blood clots of similar sizes.

(2) Grouping

Two groups, nanoprobe group and blocking group were established to verify the targeting ability. In the blocking group, the blood clots were pretreated with excessive CREKA (CREKA:IR806-PDA@BSA-CREKA = 100:1) for 1 h to consume binding sites, while no pretreatment was conducted in nanoprobe group. Then corresponding concentrations of IR806-PDA@BSA-CREKA (0, 2.5, 5, 10, 20, 50 μg mL^{-1}) were respectively added into two groups and incubated with the blood clots for 2 h at room temperature. After the incubation, the blood clots were washed 3–4 times with PBS before NIR-II fluorescence imaging (808 mm laser, 40 mW cm^{-2}; 980 nm filter; exposure time 500 ms).

2.9.4. In vitro blood clot activation assays

The blood clots were prepared by the same method and placed in a 96-well plate. Four groups were set: nanoprobe groups (20 μg mL^{-1}, 40 μg mL^{-1}), PDI inhibitor group (20 μg mL^{-1}), pure blood clot group (PBS). In PDI inhibitor group, PDI inhibitor 16F16 was added 1 h before the incubation to inhibit the enzymatic activity of PDI. Then all groups were added with nanoprobe or PBS with blood clots, and shaken at 37 °C for discontinuous NIR-II fluorescence imaging (0, 10, 20, 30, 40, 50 min) (808 mm laser, 40 mW cm^{-2}; 980 nm filter; exposure time 500 ms).

2.10. Animals

The C57BL/6 mice (male, 6–8 week, 25–30 g) were purchased from Yangzhou University Comparative Medicine Centre. All animal procedures in this study were conducted in accordance with the Chinese National Guide for the Management and Use of Experimental Animals (GB/T 35,892–2018) approved by the animal ethics committee of Wuhan University (WP2020-08076).

2.10.1. NIR-II fluorescence imaging of anastomotic thrombosis in vivo

(1) Animal model

The anastomotic thrombosis model was constructed combining anastomosis surgery with conventional method. Firstly, C57BL/6 mice were anesthetized by isoflurane (2%), and the right carotid artery was exposed and dissected from circumferential connective tissues under the operative microscope. The blood flow being clamped, a 7-0 suture needle withsilk was used to pass through the monolayer of carotid artery and performed knot-tying suture to apply physical injury on vascular endotheliocyte, mimicking the microvascular anastomosis. Pay attention not to snag the contralateral vascular war, which would result in blood flow interruption. Then the blood flow was recovered and covered by a 1 × 2 mm filter paper filled with 6% $FeCl_3$ for 5 min. Finally, the operative filed was cleaned with saline. 5 min later, the nanoprobes were injected through the tail vein. The intensity of carotid artery of mice were tracked continuously (5 min, 30 min, 1 h, 1.5 h, 2 h, 3 h, 4 h, 5 h) by NIR-II fluorescence imaging instrument.

(2) SBR calculation

The SBR in NIR-II fluorescence imaging was calculated by software Image J. we draw a line in the region of interest (ROI), the fluorescence intensity curve across this line will be extracted, and the highest intensity was selected as the "signal" (I_{signal}). The lowest intensity was selected as the "background" ($I_{background}$). SBR was calculated as follows: SBR = $I_{signal}/I_{background}$. For each experimental group, n = 3.

(3) Grouping

Three groups were established, nanoprobe group, non-responsive group, non-targeting group. After modeling, three groups were respectively injected with IR806-PDA@BSA-CREKA (IR806-PDA 100 μg mL^{-1}, 100 μL), IR806@BSA-CREKA (IR806 100 μg mL^{-1}, 100 μL), IR806-PDA@BSA (IR806-PDA 100 μg mL^{-1}, 100 μL).

(4) Immunofluorescence (IF) staining

C57BL/6 mice with right carotid artery thrombosis were injected with 100 μL of IR806-PDA@BSA-CREKA labeled with FITC (100 μg mL^{-1}, 100 μL). After 4 h of circulation, the right carotid artery was resected, and frozen sections were generated for fibrin immunofluorescence staining. The aggregation of the nanoprobe in the thrombus site *in vivo* was observed using CLSM.

2.10.2. Carotid artery thrombolysis monitoring by NIR-II

The right carotid anastomotic thrombosis model was induced by anastomosis +6% $FeCl_3$ injury. IR806-PDA@BSA-CREKA was injected 5 min (fresh thrombus) and 3 d (old thrombus) after the thrombus formation, respectively. Thrombolytic therapy was performed in mice using 1 × PBS (pH = 7.4) with Actilyse®/Alteplase for injection [recombinant human tissue fibrinogen activator for injection (rt-PA)] solution. According to the study of Li et al. [20], rt-PA was configured with a concentration of 0.15 mg mL^{-1} and injected through the tail vein at a volume of 50 μL per animal for thrombolysis. The injection of rt-PA was conducted after the enrichment of nanoprobe, while the intensity within the carotid artery region of mice was continuously monitored by NIR-II fluorescence imaging immediately after the injection of rt-PA.

2.10.3. In vivo biodistribution and biosafety of the nanoprobe

(1) Half-life assessment.

Blood was firstly sampled as a reference before the injection of the nanoprobe, using the same heparinized capillary tubes. Then Blood samples were collected from the end of the tail of the mice administrated with IR806-PDA@BSA-CREKA (intravenous injection, 100 μL, 100 μg mL^{-1}) at 5 min, 10 min, 20 min, 30 min, 40 min, 1 h, 2 h, 4 h, 8 h, 12 h, 24 h post injection. The collected blood samples were imaged by NIR-II fluorescence imaging system (808 nm, 980 nm filter, 300 ms' exposure). According to the following equation, half-life was computed as $t_{1/2} = \ln(2)/K$:

Y=(Y$_0$ - Plateau)*exp (-K*X) + Plateau.

(2) Imaging evaluation *in vivo*

The whole body of C57BL/6 mice was imaged by NIR-II fluorescence imaging system after the injection of IR806-PDA@BSA-CREKA (100 μg mL^{-1}, 100 μL) at different time points (5 min, 10 min, 15 min, 30 min, 1 h, 1.5 h, 2 h, 2.5 h, 3 h, 6 h, 9 h, 12 h, 48 h, 72 h), excited by an 808 nm laser with power density of 40 mW cm^{-2}. Fluorescence was collected using a 980 nm filter and the exposure time was set to 100 ms.

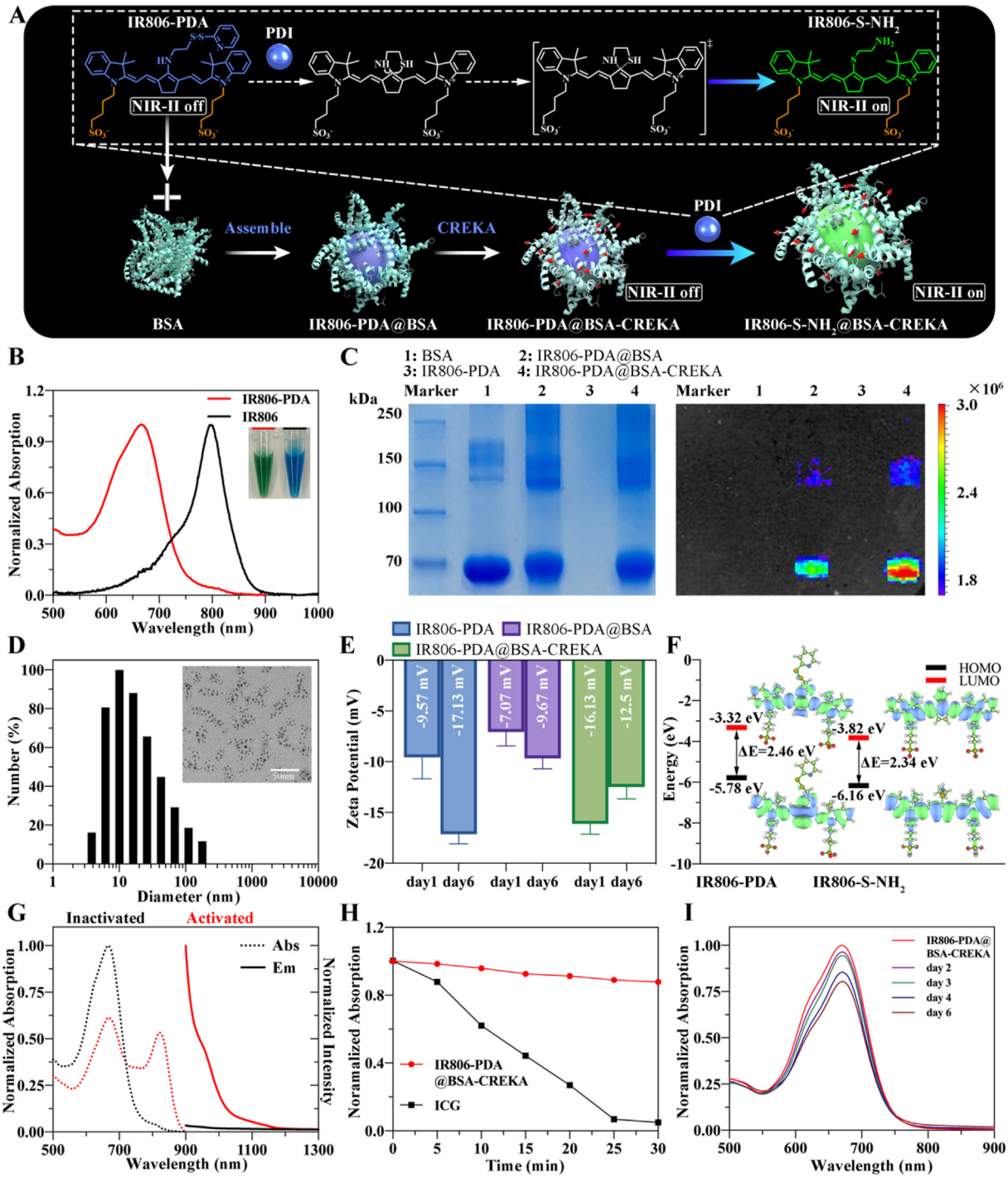

Fig. 1. Construction, identification and characterization of IR806-PDA@BSA-CREKA. **A**) Illustration of the construction and activation of the nanoprobe. **B**) The absorption spectrum and the color of IR806 and IR806-PDA. **C**) SDS-PAGE and fluorescent imaging of the gel for BSA, IR806-PDA, IR806-PDA@BSA, IR806-PDA@BSA-CREKA. (λ_{ex}: 670 nm; λ_{em}: 740 nm) **D**) Representative TEM image and DLS analysis of IR806-PDA@BSA-CREKA. Scale bar = 50 nm. **E**) Zeta Potential stability assessment of IR806-PDA, IR806-PDA@BSA, IR806-PDA@BSA-CREKA. Data were shown as mean ± SD, n = 3. **F**) Molecular orbitals of IR806-PDA before and after the activation of PDI, and calculated HOMO, LUMO and Energy gap ($\Delta E = E_{LUMO}$-E_{HOMO}). **G**) Different absorption (dotted line) and fluorescence emission (solid line) of inactivated (black) and activated (red) IR806-PDA@BSA-CREKA. **H**) Photobleaching study for IR806-PDA@BSA-CREKA and ICG. Data were shown as mean ± SD, n = 3. **I**) Absorption changes of IR806-PDA@BSA-CREKA within the 6 days' storage.

(3) Biodistribution in major organs

The major organs (heart, liver, spleen, lung and kidney) of mice were collected for NIR-II fluorescence imaging, evaluating the biological distribution of the nanoprobe. Fluorescent signals were collected using an 808 nm laser and a 980 nm filter, with an exposure time of 100 ms.

(4) Histological evaluation of *in vivo* toxicity

The major organs (heart, liver, spleen, lung and kidney) and the carotid artery of mice administrated with IR806-PDA@BSA-CREKA were resected for hematoxylin & eosin (H&E) staining at 1 d and 7 d post injection. The mice injected with PBS were taken as control.

2.11. Statistical analysis

All results were expressed as mean ± standard deviation. The experimental data *in vitro* and *in vivo* were analyzed using the Two-way analysis of variance (Two-way ANOVA) statistical comparison among different groups at different time points. Differences at the 95% confidence level ($p < 0.05$) were considered to be statistically significant ($p < 0.05$, *; $p < 0.01$, **; $p < 0.001$, ***; $p < 0.0001$, ****).

3. Results and discussion

3.1. Synthesis and characterization of IR806-PDA

Currently, the development of photosensitizer (PS) for redox imbalances and a PS-based nanoplatform are hot topics in molecular imaging [37]. In general, reduction-responsive PS is designed based on several mechanisms, including Michael addition [38], cleavage of sulfonamides and sulfonates [39], mercaptan halogen nucleophilic substitution [40], and disulfide bond cleavage [41]. Inspired by this, considering the disulfide isomerism of PDI and the reductase activity of thrombus-related PDI, a reduction-responsive PS, IR806-PDA was prepared through amino-halogen nucleophilic substitution. As shown in Fig. S1A, the active chlorine on IR806 was substituted by the amino group on the thiol-activable disulfidipyridine (-S-S-PDA) in presence of triethylamine (TEA). Then the nanoprobe was constructed based on the assemble of BSA and IR806-PDA (Fig. 1A), followed with conjugation of fibrin targeting peptide CREKA with the assembled supramolecular complex IR806-PDA@BSA (Fig. S1B). When treated with PDI, the disulfide on disulfidipyridine can be broken and reduced to sulfhydryl (-SH) by the extrusion of pyridine. The subsequent exchange between –SH and secondary amine formed thiolate substituted IR806 (IR806-S-NH_2), which exhibited a significant redshift new absorption peak, as illustrated in Fig. 1A. The different absorption of the IR806-S-NH_2 compared with IR806-PDA permit the construction of a cyanine derivative-based activatable nanoprobe. During the process of reaction, the color of the solution gradually changed from green (IR806) to blue (IR806-PDA) (Fig. 1B), preliminarily indicating the successful substitution. The structure of substituted products was characterized by proton nuclear magnetic resonance (^{1}H NMR) (Fig. S2). The results of matrix assisted laser desorption ionization-time of flight mass spectrometry (MALDI--TOF-MS) (Fig. S3) showed that the mass peak of IR806-PDA located at 826.992 *m/z*. Combining the results of ^{1}H NMR, MALDI-TOF-MS and the changes of Ultraviolet and visible (UV–vis) absorption spectra of IR806 (peak at 797 nm) and IR806-PDA (peak at 658 nm) (Fig. 1B), the synthesize of IR806-PDA was confirmed. The absorption spectra of IR806-PDA of different concentrations in 1 × PBS (pH = 7.4) were recorded with the UV–visible spectrometer, and the results showed that the absorption peaked at 658 nm (Fig. S4A). Then a standard curve was fitted according to the absorbance at 658 nm of IR806-PDA at different concentrations (Fig. S4B). In the subsequent experiments, the concentration of IR806-PDA will be taken as the concentration of the nanoprobe, determined by the linear relationship: Y = 0.01244*X+0.04813.

3.2. Construction of targeted activatable NIR-II nanoprobe IR806-PDA@BSA-CREKA

Cyanine dye is characterized with rapid hepatobiliary clearance *in vivo* and high biocompatibility. However, the universal application of cyanine in bioimaging and in clinic is limited by its instability, high photon attenuation, tissue autofluorescence and light scattering [28]. Protein-based supramolecular biomaterials have been extensively investigated [42], benefited from their satisfactory biocompatibility, safe degradability [43], and importance role in stabilizing nanoparticles and improving material properties through supramolecular interactions [44]. Conjugated individually to supramolecular blocks by the non-covalent action, nanoprobes can be optimized in several aspects, including excretory pathway, pharmacokinetic [45], even improved QYs [28]. As Tian et al. reported, the nanomolar binding affinity interactions between cyanine dyes and albumin improved QYs by enhanced the twisted intramolecular charge transfer (TICT) processes [28]. In this study, we assembled the cyanine derivative IR806-PDA with BSA, aiming to construct a more stable supramolecular complex IR806-PDA@BSA, with brighter fluorescence emission tailing to NIR-II region. Moreover, IR806-PDA@BSA was functionally decorated with peptide CREKA to endow the nanoparticles with fibrin-targeted ability. SDS polyacrylamide gel electrophoresis (SDS-PAGE) analysis and NIR-I fluorescence imaging were applied to confirm the successful assembling of the supramolecular complexes. As shown in Fig. 1C, the protein bands of BSA, IR806-PDA@BSA and IR806-PDA@BSA-CREKA all located at around 70 kDa, but only the bands of IR806-PDA@BSA and IR806-PDA@BSA-CREKA had NIR-I fluorescence emission (λ_{ex}: 670 nm; λ_{em}: 740 nm). Whereas the band of IR806-PDA (Mw = 862.2) cannot be found within 70–250 kDa. Then spherical morphology of the nanoparticles was characterized by TEM, while diameters were determined by DLS to be 16.60 ± 1.84 nm, which was consistent with the results of TEM (Fig. 1D). The hydrodynamic diameters of IR806-PDA@BSA-CREKA dispersed in phosphate buffer solution (PBS) and 10% fetal bovine serum (FBS) were tracked using DLS and did not show obvious changes in average diameters after storage for 7 days (Fig. S5). The zeta potential of IR806-PDA, IR806-PDA@BSA, IR806-PDA@BSA-CREKA were respectively −9.57 ± 1.73 mV, −7.07 ± 1.12 mV, −16.13 ± 0.82 mV (Fig. 1E). After 6 days' storage, only the zeta potential of IR806-PDA significantly changed, from −9.57 mV to −17.13 mV, demonstrating a better structural stability of BSA-based supramolecular complexes.

The proposed NIR-II fluorescence "turn on" mechanism was investigated by theoretical calculation. As shown in Fig. 1F, the energy gap ($\Delta E = E_{LUMO}$-E_{HOMO}) decreased from 2.46 eV (IR806-PDA) to 2.34 eV (IR806-S-NH_2) after the activation of PDI, which can contribute to a redshift absorption spectrum. Thus, the photophysical behaviors of IR806-PDA@BSA-CREKA were further investigated in Fig. 1G. Before being activated, IR806-PDA@BSA-CREKA showed an intense absorbance around 666 nm, the spectrum of which had a slightly redshift compared with IR806-PDA alone. Whereas the activated product, IR806-S-NH_2@BSA-CREKA emerged with an absorption peak at 821 nm. Excited by an 808 nm laser, IR806-PDA@BSA-CREKA had no fluorescence emission in NIR-II window, while IR806-S-NH_2@BSA-CREKA displayed intense fluorescence emission at 963 nm and extended in NIR-II region. Photobleaching study were performed to compare the photostability of commercial cyanine dye ICG, with cyanine derivative@BSA complexes. After 30 min' irradiation of 635 nm laser, the absorbance of IR806-PDA@BSA-CREKA only decreased to 87.7% compared to that of 0 min, while the absorbance of ICG dropped to 5% of the initial absorbance (Fig. 1H). As shown in Fig. S6A, IR806-PDA exhibited time-dependent absorption decrease in aqueous solution. After 6 days' storage, the absorption of IR806-PDA at 655 nm had dropped by 43.6%, and the waveform had already changed on day 2. In the form of supramolecular complex, IR806-PDA@BSA and IR806-PDA@BSA-CREKA only showed slight decrease at day 6 (Figs. S6B and 1I). These results indicated superior stabilities of BSA-based supramolecular complexes compared with

cyanine or cyanine derivative.

3.3. IR806-PDA@BSA-CREKA target to fibrin and respond to PDI in vitro

In general, thrombus-related PDI is secreted by activated platelets and endothelial cells [46], with reducing enzymatic activity, while negligible amount of PDI exists in plasma and on rest platelets in redox homeostasis. Thus, PDI can be recognized as a key biomolecular event for fresh thrombosis since it plays a role in maintaining the balance of oxidation/reduction states of disulfide bonds of hemostatic proteins in the process of thrombus formation *in vivo* [47]. In our study, PDI was innovatively chosen as the stimulating factor for the activatable probe and the responsiveness to PDI was firstly explored. The absorption and emission spectrum were respectively recorded before and after incubation with PDI. Since PDI must maintain its reduced form to exhibit its enzyme activity [13], dithiothreitol (DTT), a mercaptan cofactor, was added before incubation to mimic the physiological environment *in vivo*. The absorbance showed PDI-concentration-related and time-dependent changes (Fig. 2A and B), with an elevating absorption peak at 821 nm. The absorbance-concentration and absorbance-time related curves were fitted. Similarly, the fluorescence emission of PDI-activated nanoprobes were tested, and fluorescence increased in PDI-concentration- and incubation time-dependent manners (Fig. 2C and D). The intensity-concentration and intensity-time correlated curves were also

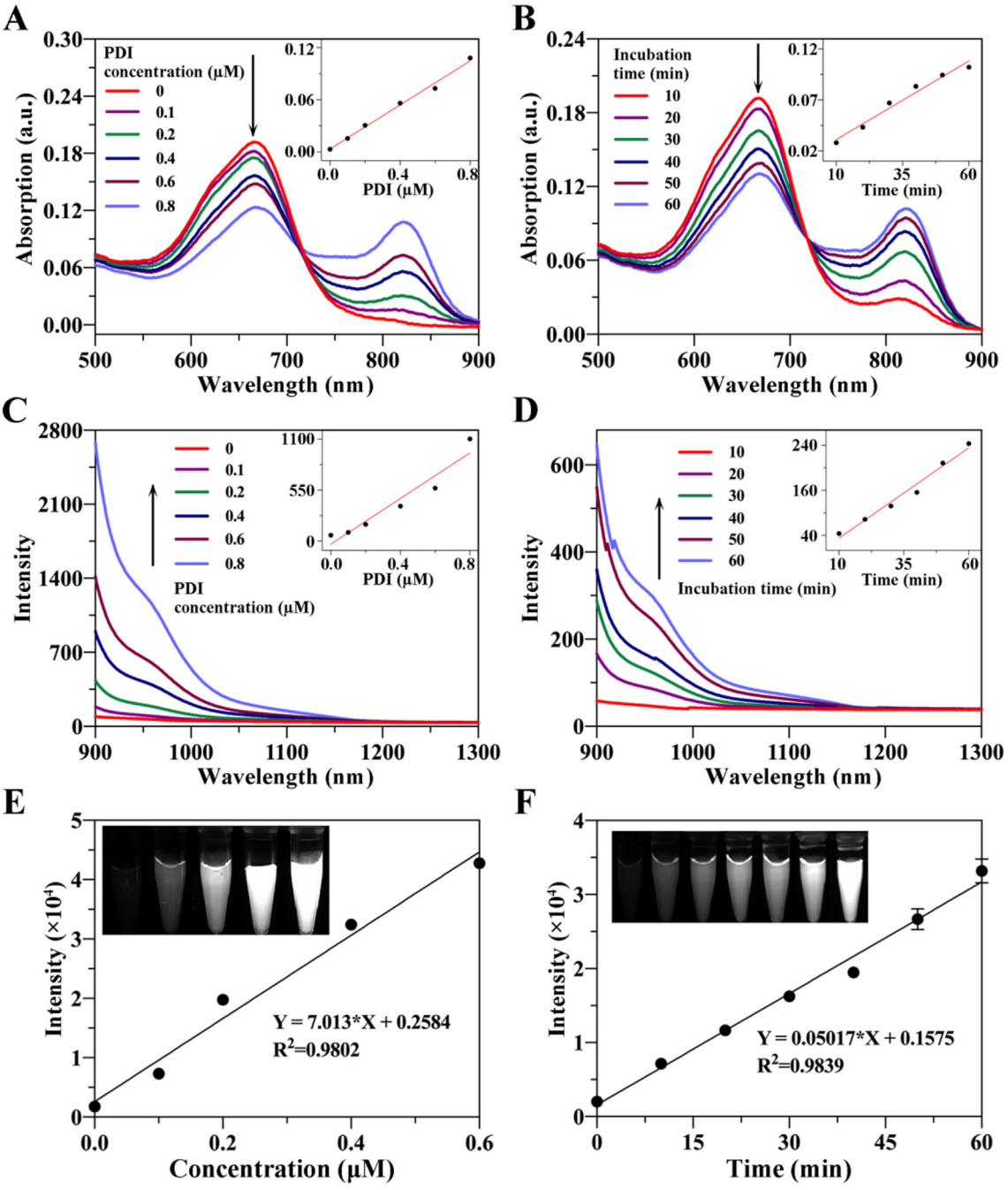

Fig. 2. Responsiveness of IR806-PDA@BSA-CREKA to PDI. **A**) Absorption changes of nanoprobe when incubated with different concentrations of PDI (0, 0.1, 0.2, 0.4, 0.6, 0.8 μM) for 1 h. **B**) The absorption spectrums of the nanoprobe recorded at different time (10, 20, 30, 40, 50, 60 min) after the incubation with 0.8 μM of PDI. Fluorescence emission variation of the nanoprobe added with different concentrations of PDI (0, 0.1, 0.2, 0.4, 0.6, 0.8 μM) after 1 h (**C**) or with 0.8 μM of PDI for different time (10, 20, 30, 40, 50, 60 min) (**D**), and corresponding NIR-II fluorescence images (**E, F**). Data were shown as mean ± SD, n = 3.

fitted according to the fluorescence intensities at 963 nm. A NIR-II fluorescence imaging system with an 808 nm laser equipped with 980 nm filter were applied to verify the imaging ability of IR806-PDA@BSA-CREKA. As shown in Fig. 2E and F, activated by PDI, the nanoprobe was suitable for NIR-II fluorescent imaging.

To elaborate the specificity activation of IR806-PDA@BSA-CREKA to PDI, the fluorescence intensity changes of the nanoprobe incubated with physiological components including several amino acid and enzymes (PDI, proline, lysine, aspartic acid, arginine, histidine, threonine, tyrosine, tryptophan, thrombin, glutathione) were evaluated and only PDI-activated nanoprobe presented impressive fluorescence emission (Fig. S7), illustrating the specific activation of IR806-PDA@BSA-CREKA to PDI.

To realize the early positive visualization of anastomosis thrombosis, both the targeted ability to fibrin and the responsiveness to PDI of IR806-PDA@BSA-CREKA need to be assessed *in vitro*. To distinguish fresh and fibrinolytic thrombus from old/non-fibrinolytic ones, fibrin targeting becomes an essential step. Thus, the pentapeptide CREKA was decorated onto the surface of nanoprobe to endow it with fibrin-targeting ability. To identify this, blood clot was established using the whole blood of mice and let it coagulate in 96 well plate itself, mimicking the blood clot forming process *in vivo*. Blood clots of similar weights were incubated with different concentrations of IR806-PDA@BSA-CREKA for 2 h and the remanent nanoprobe was washed off. Those nanoprobes targeted to the blood clots would not be washed off and light up the clots. As shown in Fig. 3A, the blood clots with concentration-dependent NIR-II fluorescent intensity increase indicated the targeting ability of IR806-PDA@BSA-CREKA. To further verify the targeting role of CREKA, a blocking group was set, in which blood clots were incubated with excess CREKA (100:1) beforehand to consume the peptide binding sites, and displayed significantly decreased fluorescence intensities compared with that of the unblocked group (Fig. 3B) ($p < 0.0001$, ****; Two way ANOVA). These results demonstrated the CREKA-driven targeting ability of the nanoprobe to blood clots.

Next, we attempted to use blood clot to activate IR806-PDA@BSA-CREKA and the role of PDI in the activation was explored. Muller-Calleja et al. [48] had proved the inhibitory effect of 16F16 on PDI, so it was utilized as the PDI inhibitor in our study. Different concentrations of IR806-PDA@BSA-CREKA were incubated with blood clots of similar weights and saw an intensity elevation within 50 min (Fig. 3C). In contrast, when PDI inhibitor was applied before the incubation, significantly diminished fluorescence signals were detected (Fig. 3D) ($p < 0.0001$, ****; Two way ANOVA), indicating that IR806-PDA@BSA-CREKA was activated by PDI in the fresh blood clot. Results mentioned above suggested IR806-PDA@BSA-CREKA a suitable nanoprobe for fibrin-targeted and PDI-responsive NIR-II fluorescence imaging for anastomosis thrombosis.

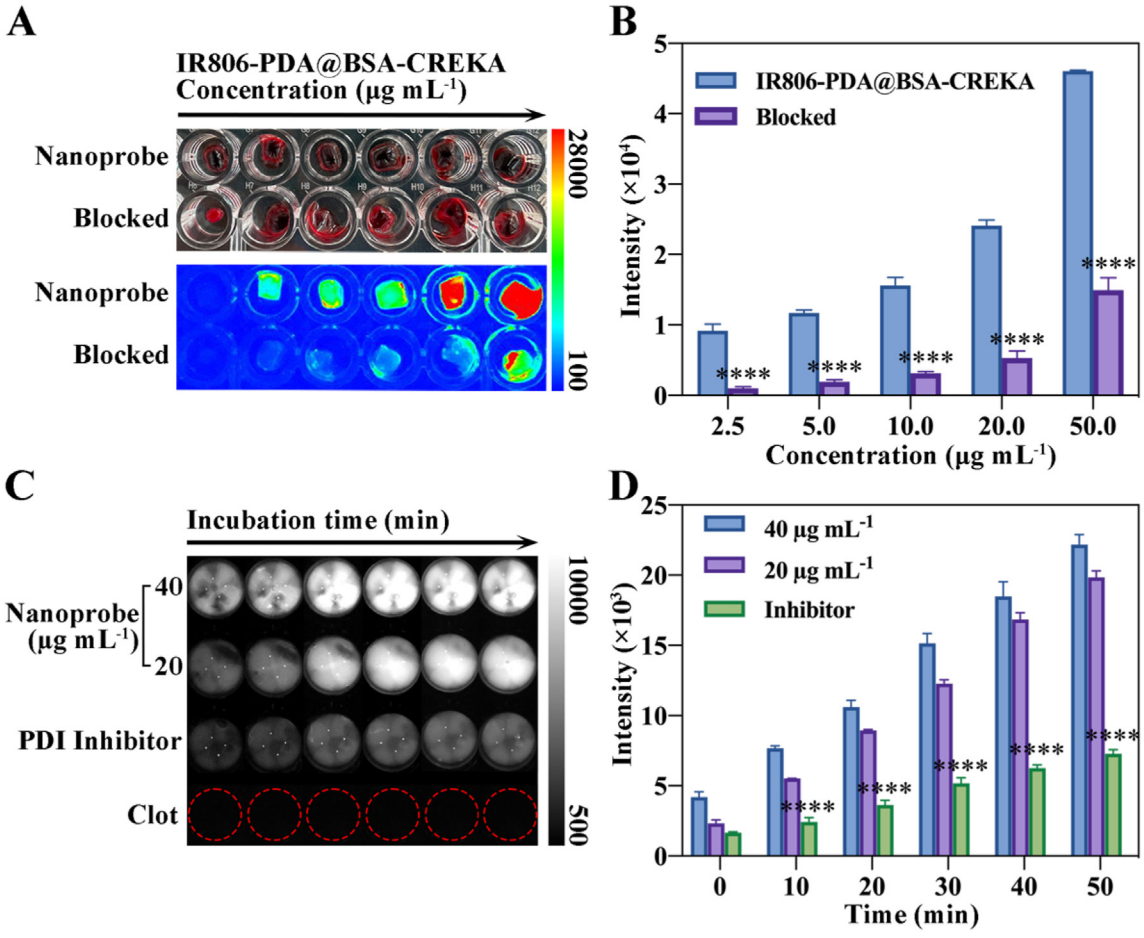

Fig. 3. Responsiveness and targeted ability to blood clot of the nanoprobe. **A**) Mice blood clots were lightened by IR806-PDA@BSA-CREKA (upper row) while the NIR-II fluorescence was significantly diminished when blocked by excessive CREKA (100:1) (lower row), and the differences of the fluorescent intensities among two groups were statistically significant (**B**) ($p < 0.0001$, ****; Two way ANOVA). Data were shown as mean ± SD, n = 3. **C**) Incubated with mice blood clots, IR806-PDA@BSA-CREKA (20, 40 μg mL^{-1}) could be activated and exhibited concentration-dependent NIR-II fluorescence (first and second rows). But the fluorescence was inhibited by PDI inhibitor 16F16 (third row) While negligible fluorescent intensity was observed in pure clots (forth row). **D**) The NIR-II fluorescent signals were collected and analyzed, demonstrating a significant decrease of fluorescent intensities in the group which was pretreated with PDI inhibitor compared to those without utility of PDI inhibitor ($p < 0.0001$, ****; Two way ANOVA). Data were shown as mean ± SD, n = 3.

3.4. IR806-PDA@BSA-CREKA for the visualization of anastomosis thrombosis

Encouraged by the results *in vitro*, the potential of IR806-PDA@BSA-CREKA used in anastomosis thrombosis NIR-II fluorescence imaging was investigated *in vivo*. Right carotid artery anastomotic thrombosis models were established by vascular anastomosis accompanied with $FeCl_3$ injury (Fig. 4A), mimicking the formatting process in anastomotic surgeries. NIR-II fluorescence imaging was performed immediately after the injection of IR806-PDA@BSA-CREKA via the tail vein, tracking the fluorescent signals within the region of thrombus. As shown in Fig. 4B, first row, the nanoprobe accumulated within the thrombus rapidly and the anastomotic thrombosis was visualized within 1 h–1.5 h. The fluorescence intensity peaked at 3 h post injection, revealing the fast activation and imaging ability of IR806-PDA@BSA-CREKA, which is of particular importance in early thrombosis detection. Moreover, with the formation and evolution of the thrombus, the newly formed ones could be continuously lighted by the nanoprobe. It was found that the shape of the thrombus kept changing, from the initial cylindrical shape to the following 'tailing' shape, representing the continuous formation of thrombosis, which was consistent with the evolution process in human, demonstrating the high sensitivity of the nanoprobe. Efforts have been made to maximize target fluorescent signals and minimize background signals, in an attempt to improve SBR, which as a result contribute to optimized sensitivity and specificity in disease diagnosis and monitoring. In contrast to "always on" fluorescence probes, activable probes do not have invariable background signals that exist in "always on" probed based imaging [49]. Thus, the SBR of IR806-PDA@BSA-CREKA applied in anastomosis thrombosis NIR-II fluorescence imaging was quantitatively investigated. In this study, the SBR was calculated using the fluorescent intensities collected in the region of thrombosis at each timepoints, and reached a maximum of 9.30 ± 0.34 at 3 h post injection (Fig. 4C, red line). These findings recommended the nanoprobe a candidate for thrombosis fast visualization and dynamical tracking.

In order to provide further data support for the responsiveness and targeting ability of IR806-PDA@BSA-CREKA to thrombosis *in vivo*, non-responsive and non-targeting groups were set for comparative evaluation. In the non-responsive group and non-targeting group, same effective concentrations of IR806@BSA-CREKA (IR806 was allocated to 100 μg mL^{-1}) and IR806-PDA@BSA (IR806-PDA was allocated to 100 μg mL^{-1}) were respectively injected through the tail vein, and NIR-II imaging was performed under the same condition. The fluorescence signal of carotid artery thrombosis in non-responsive group mice also rose within 1.5 h, but stopped rising after 2 h (Fig. 4B, second row), with a highest SBR of 2.17, which was significantly lower than that in experimental group (Fig. 4C, blue line) ($p < 0.0001$, ****; Two-way ANOVA). It suggested that responsive nanoprobe greatly improved the SBR for imaging target, and permitted higher sensitivity and better accuracy. On the other hand, in the non-targeting group, the accumulation of IR806-PDA@BSA in thrombus was relatively slower than those in other two groups and the thrombosis could not be clearly identified until 4 h after the injection (Fig. 4B, third row). This may be due to the lack of active targeting ability of IR806-PDA@BSA, where the accumulation was limited by the impaired blood flow in the narrow vascular lumen. As a result, the imaging efficiency of non-targeting probe was affected and the maximum SBR was only 3.10, showing significant differences with that of the IR806-PDA@BSA-CREKA group at 4 h (Fig. 4C, black line) ($p < 0.0001$, ****; Two-way ANOVA). A certain extent of fluorescence intensity decrease could be observed at 5 h in the non-targeting group (Fig. 4C). The limited imaging time window may also explain the restricted SBR in this group.

Comparing the SBR among three groups, IR806-PDA@BSA-CREKA exhibited significant higher SBR during 1.5 h–5 h. The results above illustrated that, in the anastomotic thrombosis imaging, IR806-PDA@BSA-CREKA was characterized with high contrast, high sensitivity, high imaging efficiency and wide imaging time window, which is suitable for accurate imaging and diagnosis for early anastomotic thrombosis, especially for the diagnosis of those micro-thrombus that are difficult to be identified by traditional imaging techniques based on anatomical changes.

To further determine the distribution of IR806-PDA@BSA-CREKA in the thrombus, fluorescein isothiocyanate (FITC) were doped into the nanoparticles as the fluorescence producer at the wavelength of 520–530 nm for confocal imaging. The carotid artery with thrombosis enriched with IR806-PDA@BSA-CREKA was resected and then co-stained with DAPI for nuclei, anti-fibrin antibody labeled by Cy3 for fibrin composition in the thrombus. Confocal laser scanning microscopy (CLSM) imaging results revealed that the fluorescent signal of FITC embedded in IR806-PDA@BSA-CREKA (green) was highly coincident with that of the fibrin (red) (Fig. 4D), illustrating the fibrin-targeting ability of nanoprobe from histological level. Moreover, regions of interest (ROI) were selected in the overlay image of thrombus and analyzed using Image J software. The scatter plots (Fig. 4E), accompanied with the calculated Pearson's correlation factors: 0.620 ± 0.124 and Manders' colocalization coefficients: 0.762 ± 0.213 (red) and 0.748 ± 0.116 (green) further confirmed the colocalization of nanoprobe and fibrin in the thrombus. Taken together, the above results validated the fast activation and efficient imaging ability of the fibrin-targeted IR806-PDA@BSA-CREKA for anastomotic thrombosis *in vivo*, and validated the capability of the nanoprobe in dynamic visualized diagnosis for thrombosis.

3.5. IR806-PDA@BSA-CREKA used for monitoring of fibrinolysis of fibrinolytic thrombus

Based on the sensitivity and fast imaging ability of IR806-PDA@BSA-CREKA revealed in anastomotic thrombosis imaging, it was further investigated in carotid thrombolysis monitoring. Fresh thrombus and old thrombus models were respectively established in mice and followed by IR806-PDA@BSA-CREKA injection. After the accumulation of nanoprobe (2–3 h post injection), clear and bright NIR-II fluorescent signal in the carotid region could be found in both groups. Fibrinolytic drug, rt-PA was systemically administrated and NIR-II fluorescence imaging was conducted to dynamically monitor the development of thrombolysis. As shown in Fig. 5A and Supplementary Video 1 and Supplementary Video 2, the NIR-II fluorescent signal of fresh thrombus decreased rapidly after the injection of rt-PA, and almost disappeared within 15 min, indicating that IR806-PDA@BSA-CREKA was capable of monitoring the fibrinolysis process. In contrast, the fluorescent signal of old thrombus has negligible changed during 20 min, reflecting that the thrombus was not fibrinolytic. The fluorescence intensities of the thrombus were standardized based on the 0 min intensity, and the change of intensities in fresh and old ones were compared (Fig. 5B). From the 3 min of fibrinolysis, there was a significant difference between the fresh and old groups ($p < 0.0001$, ****; Two-way ANOVA). The difference not only proved the higher thrombolytic efficiency in fresh thrombus, but also demonstrated that with the use of IR806-PDA@BSA-CREKA, the change of thrombus in the process of thrombolysis could be sharply captured by NIR-II fluorescence imaging. The H&E staining of the carotid artery also confirmed the success thrombolysis of the fresh thrombus (Fig. S8A), while the old thrombus did not show apparent thrombolytic degradation (Fig. S8B), which was consistent with the development of thrombus components. Therefore, the utility of IR806-PDA@BSA-CREKA permits dynamic monitoring for thrombolysis and can identify the fibrinolytic fresh thrombus, characterized with high contrast and high sensitivity.

Supplementary video related to this article can be found at https://doi.org/10.1016/j.mtbio.2023.100697

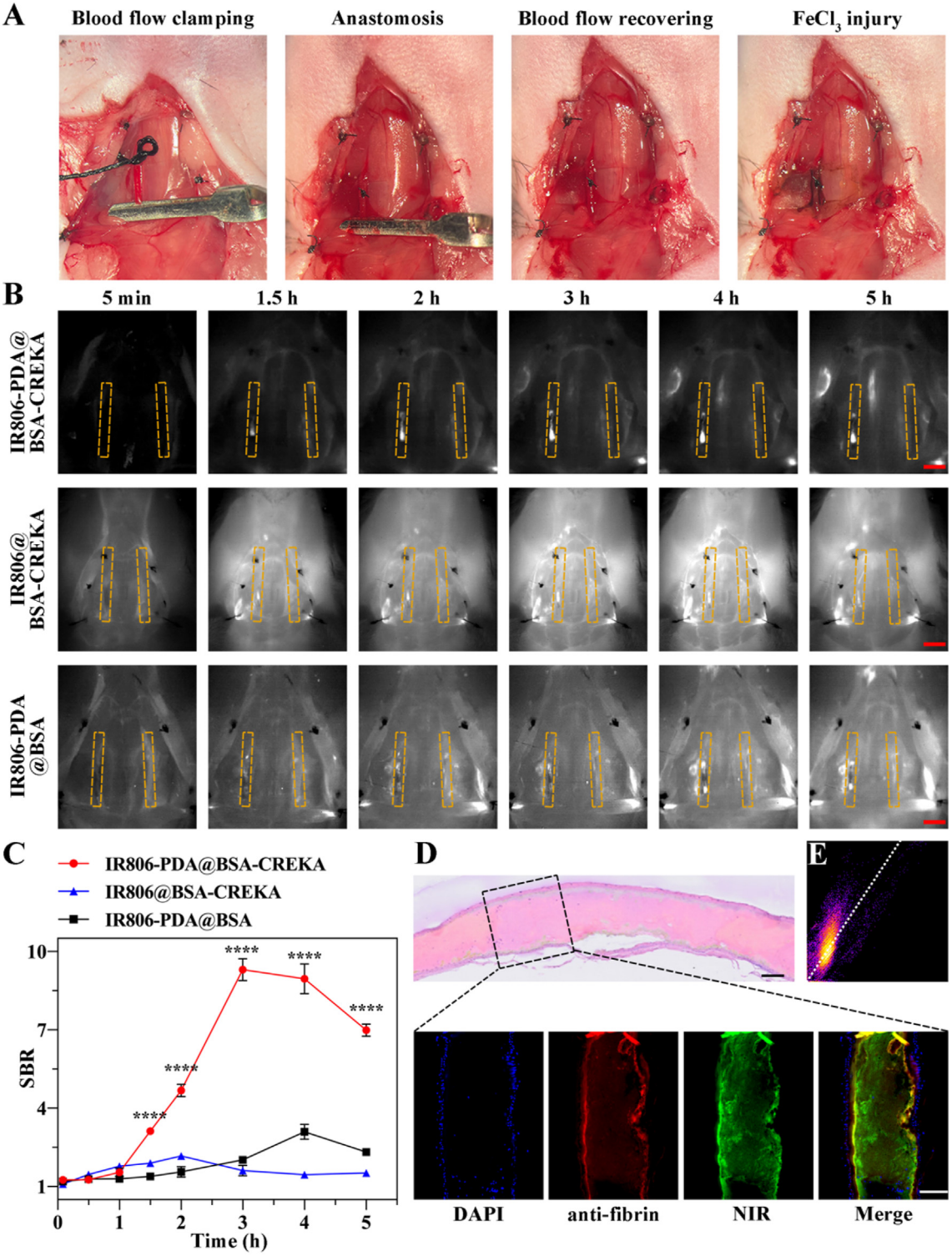

Fig. 4. In vivo NIR-II fluorescence imaging of anastomotic thrombosis using IR806-PDA@BSA-CREKA. **A)** Schematic illustration of the surgical modeling process of right carotid artery anastomotic thrombosis models in mice. **B)** NIR-II fluorescence images of right carotid artery anastomotic thrombosis in mice injected with IR806-PDA@BSA-CREKA (100 μg mL^{-1}, 100 μL; first row), IR806@BSA-CREKA (100 μg mL^{-1}, 100 μL; second row) and IR806-PDA@BSA (100 μg mL^{-1}, 100 μL; trird row) at different time post injection (5 min, 1.5 h, 2 h, 3 h, 4 h, 5 h). Scale bar: 2 mm. **C)** Monitoring of SBR in accordance with the NIR-II fluorescence intensities collected within the thrombus region (yellow dotted rectangle in (**B**)) ($p < 0.0001$, ****; Two-way ANOVA). Data were shown as mean ± SD, n = 3. **D)** CLSM results of carotid artery thrombosis in mice injected with FITC labeled IR806-PDA@BSA-CREKA accompanied with immunofluorescent staining using Cy3 labeled anti-fibrin antibody. DAPI (blue): λ_{ex}: 364 nm , λem: 454 nm; FITC (green): λex: 490 nm , λem: 520 nm; Cy3 (red): λex: 552 nm , λ_{em}: 565 nm. Scale bar: 100 μm. **E)** Colocalization analysis result for the CLSM image in (**D**).

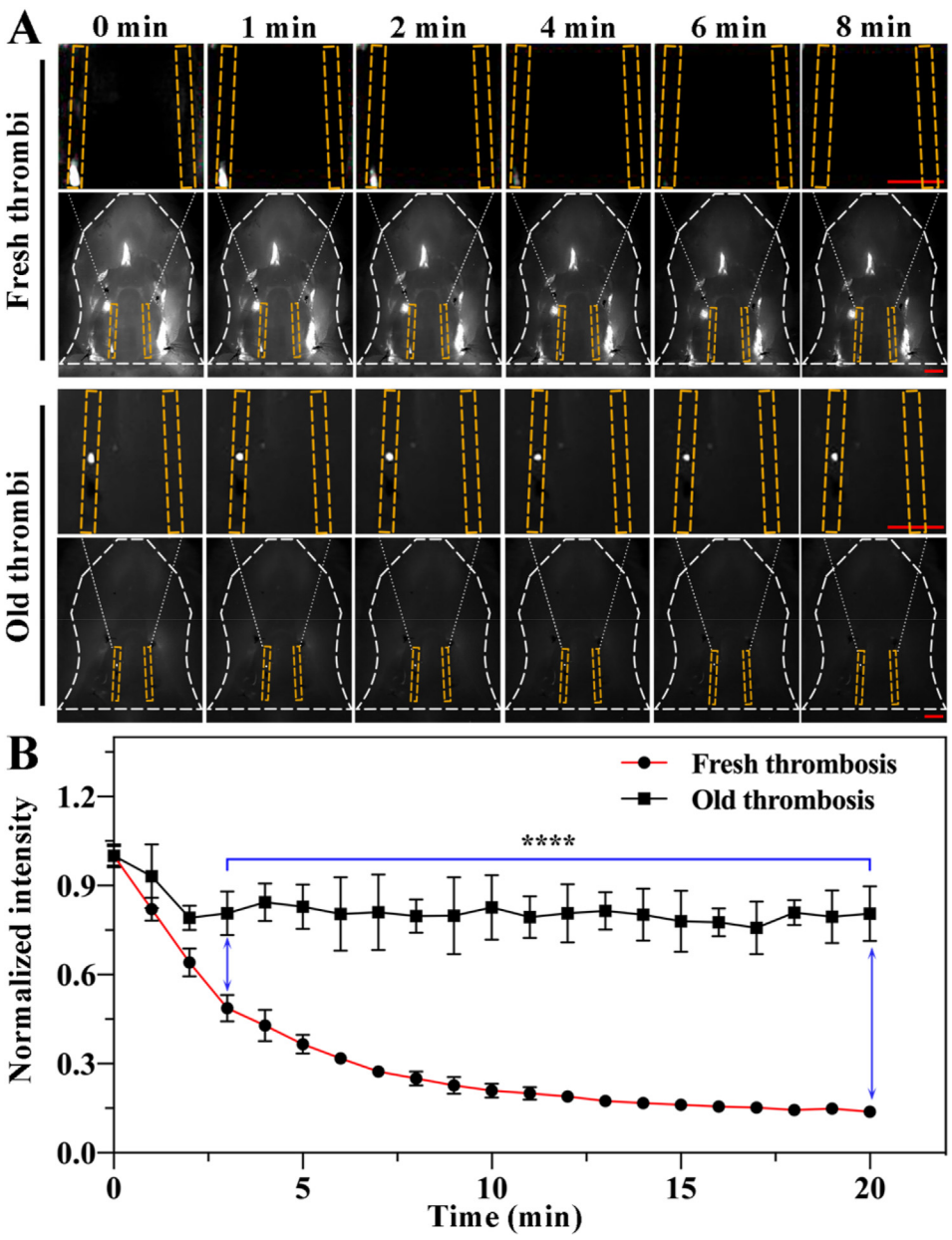

Fig. 5. NIR-II fluorescence imaging for thrombolysis of the right carotid artery thrombosis in mice. **A**) Dynamic monitoring for thrombolysis of fresh (upper) and old (lower) right carotid artery thrombosis models using IR806-PDA@BSA-CREKA (100 μg mL^{-1}, 100 μL). Scale bar: 2 mm. **B**) The NIR-II fluorescence intensities collected within the thrombus region (yellow dotted rectangle in (**A**)) were collected and normalized to evaluation the changes with the thrombolysis process between fresh and old thrombus groups ($p < 0.0001$, ****; Two-way ANOVA). Data were shown as mean ± SD, n = 3.

3.6. *In vivo metabolism, distribution and biotoxicity assessments of IR806-PDA@BSA-CREKA*

As an ideal biomedical nanoprobes, decent biocompatibility and low toxicity are critical for further potential clinical application. Cytotoxicity assays were performed in NIH3T3 cells and in RAW264.7 cells incubated with IR806-PDA@BSA-CREKA for 24 h, and revealed little cell viability decrease at the concentration of 60 μg mL^{-1} (Fig. S9), suggesting its low cytotoxicity. The biocompatibility of IR806-PDA@BSA-CREKA *in vivo* was also assessed. Briefly, the biodistribution of the nanoprobe was tracked using NIR-II fluorescence imaging after tail vein injection. Results in Fig. 6A revealed that IR806-PDA@BSA-CREKA was mainly excreted through the urinary system, whereas IR806-PDA was mainly metabolized by the liver. Both of them showed high metabolic efficiency since there was negligible residual fluorescent signal in the body of mice at 24 h post injection. In addition, the metabolic efficiency of the nanoprobe was evaluated by collecting blood serum from the end of tail of the mice and NIR-II fluorescence imaging exhibited the metabolic process in the serum. The fluorescence intensity at each time points were nonlinearly fitted and calculated to get the half-life time of the nanoprobe to be only 9 min (Fig. 6B). It showed that the nanoprobe had high blood metabolism efficiency and there was no problem of nano material retention and no hidden danger in biological safety. At the same time, the mice were sacrificed at different time points after the injection and the fluorescence of major organs including heart, liver, spleen, lung, kidney were collected by NIR-II fluorescence imaging, so as to investigate the biodistribution in organs *ex vivo*. As presented in Fig. S10A and Fig. S10B, the fluorescence in liver and kidney reached the highest at 3 h and decreased rapidly within 24 h. At 48 h–72 h, there was almost no residual fluorescence in all organs, which was consistent with the results of NIR-II fluorescence imaging *in vivo*. The mice administrated with IR806-PDA@BSA-CREKA was sacrificed at 1 d and 7 d for harvesting the major organs. The histological staining of the organs showed no obvious tissue necrosis or inflammation *in vivo* (Fig. 6C). In general, these results confirmed the low toxicity and favorable biocompatibility of IR806-PDA@BSA-CREKA *in vitro* and *in vivo*.

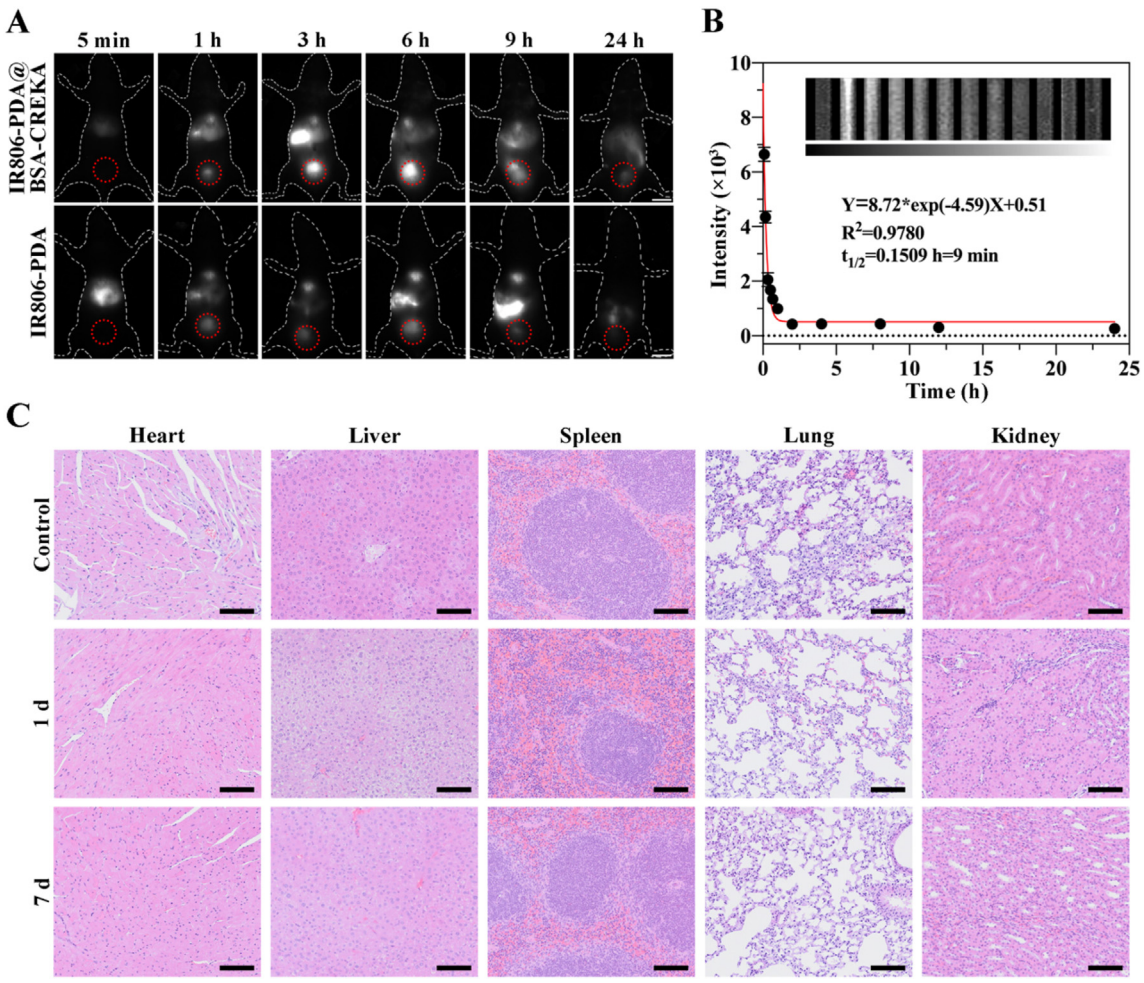

Fig. 6. *In vivo* metabolism, distribution and biotoxicity assessments of IR806-PDA@BSA-CREKA. **A**) Dynamic monitoring of the whole body of mice injected with IR806-PDA@BSA-CREKA (100 μg mL^{-1}, 100 μL) to observe the metabolism of nanoprobe *in vivo*. Scale bar: 1 cm. **B**) Calculation of half-life of IR806-PDA@BSA-CREKA *in vivo* based on NIR-II fluorescence intensities of blood collected from the tail of mice at different timepoints (5 min, 10 min, 20 min, 30 min, 40 min, 1 h, 2 h, 4 h, 8 h, 12 h, 24 h) post injection. Data were shown as mean ± SD, n = 3. **C**) H&E staining of major organs (heart, liver, spleen, lung, kidney) excised from mice at 1 d and 7 d after the systemic administration of IR806-PDA@BSA-CREKA (100 μg mL^{-1}, 100 μL). Scale bar: 200 μm.

4. Conclusion

We have constructed a targeted and activatable NIR-II nanoprobe based on the supramolecular complex of cyanine derivatives and BSA, namely IR806-PDA@BSA-CREKA. It is characterized with water solubility, small particle size and high stability. IR806-PDA@BSA-CREKA can be activated by protein disulfide isomerase, exhibiting longer absorption and NIR-II fluorescence emission. The nanoprobe shows responsiveness and targeting ability to blood clots *in vitro*. Simultaneously, accurate NIR-II visualized diagnosis of anastomotic thrombosis, identification and dynamical monitoring of thrombolysis for fresh fibrinolytic thrombus can be realized by the nanoprobe. The nanoprobe has favorable biocompatibility, with negligible cytotoxicity, being excreted through renal metabolic pathway, and shows no obvious organ toxicity. Based on a novel biomolecular event, activated PDI in fresh thrombosis, our supramolecular complex-based NIR-II nanoprobe provides an alternative for early diagnosis for anastomotic thrombosis and a safe real-time monitoring for thrombolysis therapies, simultaneously contributes a revolted strategy for guiding the therapeutic selection between thrombolysis and thrombectomy for thrombosis treatment in clinic.

Credit author Statement

Ying Yuan: Conceptualization, Methodology, Investigation, Writing - Original Draft, **Shanchao Diao:** Methodology, Investigation, Writing - Original Draft, **Dong Zhang:** Software, Investigation, **Wanrong Yi:** Investigation, **Baiwen Qi:** Investigation, **Xiang Hu:** Investigation, **Chen Xie:** Writing - Review & Editing, Supervision, Funding acquisition, **Quli Fan:** Methodology, Writing - Review & Editing, Supervision, **Aixi Yu:** Conceptualization, Writing - Review & Editing, Supervision, Funding acquisition.

Declaration of competing interest

The authors declare that they have no known competing financial interests or personal relationships that could have appeared to influence the work reported in this paper.

Data availability

Data will be made available on request.

Acknowledgements

Y.Y and S.D. contributed equally to this work. This study was financially supported by the National Natural Science Foundation of China (Grant Numbers: 82072440, 61905122, 22174070), and Department of Science and Technology of Hubei Province Jiebang Project (Grant Number: 2022BEC028).

Appendix A. Supplementary data

Supplementary data to this article can be found online at https://doi.org/10.1016/j.mtbio.2023.100697.

References

[1] S.M. Vartanian, M.S. Conte, Surgical intervention for peripheral arterial disease, Circ. Res. 116 (2015) 1614–1628, https://doi.org/10.1161/CIRCRESAHA.116.303504.
[2] M.D. Gerhard-Herman, H.L. Gornik, C. Barrett, N.R. Barshes, M.A. Corriere, D.E. Drachman, L.A. Fleisher, F.G. Fowkes, N.M. Hamburg, S. Kinlay, R. Lookstein, S. Misra, L. Mureebe, J.W. Olin, R.A. Patel, J.G. Regensteiner, A. Schanzer, M.H. Shishehbor, K.J. Stewart, D. Treat-Jacobson, M.E. Walsh, AHA/ACC guideline on the management of patients with lower extremity peripheral artery disease: executive summary: a report of the American college of cardiology/American heart association task force on clinical practice guidelines, Circulation 135 (2016) e686–e725, https://doi.org/10.1161/CIR.0000000000000470, 2017.
[3] J. Silvain, J.P. Collet, C. Nagaswami, F. Beygui, K.E. Edmondson, A. Bellemain-Appaix, G. Cayla, A. Pena, D. Brugier, O. Barthelemy, G. Montalescot, J.W. Weisel, Composition of coronary thrombus in acute myocardial infarction, J. Am. Coll. Cardiol. 57 (2011) 1359–1367, https://doi.org/10.1016/j.jacc.2010.09.077.
[4] Y. Zhang, G. Zhang, Z. Zeng, K. Pu, Activatable molecular probes for fluorescence-guided surgery, endoscopy and tissue biopsy, Chem. Soc. Rev. 51 (2022) 566–593, https://doi.org/10.1039/d1cs00525a.
[5] R. Zhang, J. Yong, J. Yuan, Z. Ping Xu, Recent advances in the development of responsive probes for selective detection of cysteine, Coord. Chem. Rev. 408 (2020), 213182, https://doi.org/10.1016/j.ccr.2020.213182.
[6] C. Chen, R. Tian, Y. Zeng, C. Chu, G. Liu, Activatable fluorescence probes for "Turn-On" and ratiometric biosensing and bioimaging: from NIR-I to NIR-II, Bioconjugate Chem. 31 (2020) 276–292, https://doi.org/10.1021/acs.bioconjchem.9b00734.
[7] J. Huang, K. Pu, Activatable molecular probes for second near-infrared fluorescence, chemiluminescence, and photoacoustic imaging, Angew Chem. Int. Ed. Engl. 59 (2020) 11717–11731, https://doi.org/10.1002/anie.202001783.
[8] J. Li, K. Kim, S.Y. Jeong, J. Chiu, B. Xiong, P.A. Petukhov, X. Dai, X. Li, R.K. Andrews, X. Du, P.J. Hogg, J. Cho, Platelet protein disulfide isomerase promotes glycoprotein ibalpha-mediated platelet-neutrophil interactions under thromboinflammatory conditions, Circulation 139 (2019) 1300–1319, https://doi.org/10.1161/CIRCULATIONAHA.118.036323.
[9] B. Xiong, V. Jha, J.K. Min, J. Cho, Protein disulfide isomerase in cardiovascular disease, Exp. Mol. Med. 52 (2020) 390–399, https://doi.org/10.1038/s12276-020-0401-5.
[10] J.K. Burgess, K.A. Hotchkiss, C. Suter, N.P. Dudman, J. Szollosi, C.N. Chesterman, B.H. Chong, P.J. Hogg, Physical proximity and functional association of glycoprotein 1balpha and protein-disulfide isomerase on the platelet plasma membrane, J. Biol. Chem. 275 (2000) 9758–9766, https://doi.org/10.1074/jbc.275.13.9758.
[11] J. Lahav, K. Jurk, O. Hess, M.J. Barnes, R.W. Farndale, J. Luboshitz, B.E. Kehrel, Sustained integrin ligation involves extracellular free sulfhydryls and enzymatically catalyzed disulfide exchange, Blood 100 (2002) 2472–2478, https://doi.org/10.1182/blood-2001-12-0339.
[12] J. Zhou, Y. Wu, L. Wang, L. Rauova, V.M. Hayes, M. Poncz, D.W. Essex, The C-terminal CGHC motif of protein disulfide isomerase supports thrombosis, J. Clin. Invest. 125 (2015) 4391–4406, https://doi.org/10.1172/JCI80319.
[13] G.S. Loving, P. Caravan, Activation and retention: a magnetic resonance probe for the detection of acute thrombosis, Angew Chem. Int. Ed. Engl. 53 (2014) 1140–1143, https://doi.org/10.1002/anie.201308607.
[14] C. Cui, Z. Yang, X. Hu, J. Wu, K. Shou, H. Ma, C. Jian, Y. Zhao, B. Qi, X. Hu, A. Yu, Q. Fan, Organic semiconducting nanoparticles as efficient photoacoustic agents for lightning early thrombus and monitoring thrombolysis in living mice, ACS Nano 11 (2017) 3298–3310, https://doi.org/10.1021/acsnano.7b00594.
[15] W. Sumaya, L. Wallentin, S.K. James, A. Siegbahn, K. Gabrysch, M. Bertilsson, A. Himmelmann, R.A. Ajjan, R.F. Storey, Fibrin clot properties independently predict adverse clinical outcome following acute coronary syndrome: a PLATO substudy, Eur. Heart J. 39 (2018) 1078–1085, https://doi.org/10.1093/eurheartj/ehy013.
[16] J. Xu, Y. Zhang, J. Xu, G. Liu, C. Di, X. Zhao, X. Li, Y. Li, N. Pang, C. Yang, Y. Li, B. Li, Z. Lu, M. Wang, K. Dai, R. Yan, S. Li, G. Nie, Engineered nanoplatelets for targeted delivery of plasminogen activators to reverse thrombus in multiple mouse thrombosis models, Adv. Mater. 32 (2020), e1905145, https://doi.org/10.1002/adma.201905145.
[17] W. Theiss, A. Wirtzfeld, U. Fink, P. Maubach, The success rate of fibrinolytic therapy in fresh and old thrombosis of the iliac and femoral veins, Angiology 34 (1983) 61–69, https://doi.org/10.1177/000331978303400108.
[18] B.L. Oliveira, P. Caravan, Peptide-based fibrin-targeting probes for thrombus imaging, Dalton Trans. 46 (2017) 14488–14508, https://doi.org/10.1039/c7dt02634j.
[19] C. Xu, Y. Jiang, J. Huang, J. Huang, K. Pu, Second near-infrared light-activatable polymeric nanoantagonist for photothermal immunometabolic cancer therapy, Adv. Mater. 33 (2021), e2101410, https://doi.org/10.1002/adma.202101410.
[20] B. Li, M. Zhao, L. Feng, C. Dou, S. Ding, G. Zhou, L. Lu, H. Zhang, F. Chen, X. Li, G. Li, S. Zhao, C. Jiang, Y. Wang, D. Zhao, Y. Cheng, F. Zhang, Organic NIR-II molecule with long blood half-life for in vivo dynamic vascular imaging, Nat. Commun. 11 (2020) 3102, https://doi.org/10.1038/s41467-020-16924-z.
[21] H. Li, M. Wang, B. Huang, S.W. Zhu, J.J. Zhou, D.R. Chen, R. Cui, M. Zhang, Z.J. Sun, Theranostic near-infrared-IIb emitting nanoprobes for promoting immunogenic radiotherapy and abscopal effects against cancer metastasis, Nat. Commun. 12 (2021) 7149, https://doi.org/10.1038/s41467-021-27485-0.
[22] B. Huang, T. Tang, S.H. Chen, H. Li, Z.J. Sun, Z.L. Zhang, M. Zhang, R. Cui, Near-infrared-IIb emitting single-atom catalyst for imaging-guided therapy of blood-brain barrier breakdown after traumatic brain injury, Nat. Commun. 14 (2023) 197, https://doi.org/10.1038/s41467-023-35868-8.
[23] J.L. Seifert, R.E. Connor, S.A. Kushon, M. Wang, B.A. Armitage, Spontaneous assembly of helical cyanine dye aggregates on DNA nanotemplates, J. Am. Chem. Soc. 121 (1999) 2987–2995, https://doi.org/10.1021/ja984279j.
[24] M.P. Luciano, J.M. Namgoong, R.R. Nani, S.H. Nam, C. Lee, I.H. Shin, M.J. Schnermann, J. Cha, A biliary tract-specific near-infrared fluorescent dye for image-guided hepatobiliary surgery, Mol. Pharm. 16 (2019) 3253–3260, https://doi.org/10.1021/acs.molpharmaceut.9b00453.
[25] P.C. Wu, L.Z. Guo, S. Yu, N. Zeng, Y.C. Liu, J. Yu, Z. Zhang, K. Lu, L. Sun, C. Wang, Y.H. Chang, Y.L. Lu, Y.F. Shen, S. Tai, Y.H. Chuang, J.A. Ho, K.W. Huang, Y.M. Wu, T.M. Liu, Noninvasive assessment of liver function reserve with fluorescent dosimetry of indocyanine green, Biomed. Opt Express 13 (2022) 1995–2005, https://doi.org/10.1364/BOE.446749.
[26] Y. Zou, W. Liu, W. Sun, J. Du, J. Fan, X. Peng, Highly inoxidizable heptamethine cyanine–glucose oxidase conjugate nanoagent for combination of enhanced photothermal therapy and tumor starvation, Adv. Funct. Mater. 32 (2022), 2111853, https://doi.org/10.1002/adfm.202111853.
[27] B.R. Renikuntla, H.C. Rose, J. Eldo, A.S. Waggoner, B.A. Armitage, Improved photostability and fluorescence properties through polyfluorination of a cyanine dye, Org. Lett. 6 (2004) 909–912, https://doi.org/10.1021/ol036081w.
[28] R. Tian, Q. Zeng, S. Zhu, J. Lau, S. Chandra, R. Ertsey, K.S. Hettie, T. Teraphongphom, Z. Hu, G. Niu, D.O. Kiesewetter, H. Sun, X. Zhang, A.L. Antaris, B.R. Brooks, X. Chen, Albumin-chaperoned cyanine dye yields superbright NIR-II fluorophore with enhanced pharmacokinetics, Sci. Adv. 5 (2019), https://doi.org/10.1126/sciadv.aaw0672 eaaw0672.
[29] J. Xu, T. Han, Y. Wang, F. Zhang, M. Li, L. Bai, X. Wang, B. Sun, X. Wang, J. Du, K. Liu, J. Zhang, S. Zhu, Ultrabright renal-clearable cyanine-protein nanoprobes for high-quality NIR-II angiography and lymphography, Nano Lett. 22 (2022) 7965–7975, https://doi.org/10.1021/acs.nanolett.2c03311.
[30] Q. Chen, X. Liu, J. Chen, J. Zeng, Z. Cheng, Z. Liu, A self-assembled albumin-based nanoprobe for in vivo ratiometric photoacoustic pH imaging, Adv. Mater. 27 (2015) 6820–6827, https://doi.org/10.1002/adma.201503194.
[31] Y. Liu, Z. Zhou, J. Hou, W. Xiong, H. Kim, J. Chen, C. Zheng, X. Jiang, J. Yoon, J. Shen, Tumor selective metabolic reprogramming as a prospective PD-L1 depression strategy to reactivate immunotherapy, Adv. Mater. 34 (2022), e2206121, https://doi.org/10.1002/adma.202206121.
[32] C. Yin, Y. Tang, X. Li, Z. Yang, J. Li, X. Li, W. Huang, Q. Fan, A single composition architecture-based nanoprobe for ratiometric photoacoustic imaging of glutathione (GSH) in living mice, Small 14 (2018), e1703400, https://doi.org/10.1002/smll.201703400.
[33] Y. Wu, Y. Suo, Z. Wang, Y. Yu, S. Duan, H. Liu, B. Qi, C. Jian, X. Hu, D. Zhang, A. Yu, Z. Cheng, First clinical applications for the NIR-II imaging with ICG in microsurgery, Front. Bioeng. Biotechnol. 10 (2022), 1042546, https://doi.org/10.3389/fbioe.2022.1042546.
[34] M.J. Frisch, G.W. Trucks, H.B. Schlegel, G.E. Scuseria, M.A. Robb, J.R. Cheeseman, G. Scalmani, V. Barone, B. Mennucci, G.A. Petersson, Gaussian 09, Revision D.01, Gaussian, Inc., Wallingford, C., 2016.
[35] A.D. Becke, Density-functional thermochemistry. III. The role of exact exchange, J. Chem. Phys. 98 (1993) 5648–5652, https://doi.org/10.1063/1.464913.
[36] T. Lu, F. Chen, Multiwfn: a multifunctional wavefunction analyzer, J. Comput. Chem. 33 (2012) 580–592, https://doi.org/10.1002/jcc.22885.
[37] K.K. Hershberger, A.J. Gauger, L.M. Bronstein, Utilizing stimuli responsive linkages to engineer and enhance polymer nanoparticle-based drug delivery platforms, ACS Appl. Bio Mater. 4 (2021) 4720–4736, https://doi.org/10.1021/acsabm.1c00351.
[38] D. Kand, A.M. Kalle, S.J. Varma, P. Talukdar, A chromenoquinoline-based fluorescent off-on thiol probe for bioimaging, Chem. Commun. 48 (2012) 2722–2724, https://doi.org/10.1039/c2cc16593g.
[39] I.S. Turan, F.P. Cakmak, D.C. Yildirim, R. Cetin-Atalay, E.U. Akkaya, Near-IR absorbing BODIPY derivatives as glutathione-activated photosensitizers for selective photodynamic action, Chemistry 20 (2014) 16088–16092, https://doi.org/10.1002/chem.201405450.
[40] L.Y. Niu, Y.S. Guan, Y.Z. Chen, L.Z. Wu, C.H. Tung, Q.Z. Yang, BODIPY-based ratiometric fluorescent sensor for highly selective detection of glutathione over cysteine and homocysteine, J. Am. Chem. Soc. 134 (2012) 18928–18931, https://doi.org/10.1021/ja309079f.
[41] J. Li, C. Tian, Y. Yuan, Z. Yang, C. Yin, R. Jiang, W. Song, X. Li, X. Lu, L. Zhang, Q. Fan, W. Huang, A water-soluble conjugated polymer with pendant disulfide linkages to peg chains: a highly efficient ratiometric probe with solubility-induced

fluorescence conversion for thiol detection, Macromolecules 48 (2015) 1017–1025, https://doi.org/10.1021/ma5021775.
[42] M. Cao, R. Xing, R. Chang, Y. Wang, X. Yan, Peptide-coordination self-assembly for the precise design of theranostic nanodrugs, Coord. Chem. Rev. 397 (2019) 14–27, https://doi.org/10.1016/j.ccr.2019.06.013.
[43] Y. Wang, A.G. Cheetham, G. Angacian, H. Su, L. Xie, H. Cui, Peptide-drug conjugates as effective prodrug strategies for targeted delivery, Adv. Drug Deliv. Rev. 110–111 (2017) 112–126, https://doi.org/10.1016/j.addr.2016.06.015.
[44] M. Kopp, S. Kollenda, M. Epple, Nanoparticle-protein interactions: therapeutic approaches and supramolecular chemistry, Acc. Chem. Res. 50 (2017) 1383–1390, https://doi.org/10.1021/acs.accounts.7b00051.
[45] L.Y. Rizzo, B. Theek, G. Storm, F. Kiessling, T. Lammers, Recent progress in nanomedicine: therapeutic, diagnostic and theranostic applications, Curr. Opin. Biotechnol. 24 (2013) 1159–1166, https://doi.org/10.1016/j.copbio.2013.02.020.
[46] K. Chen, T.C. Detwiler, D.W. Essex, Characterization of protein disulphide isomerase released from activated platelets, Br. J. Haematol. 90 (1995) 425–431, https://doi.org/10.1111/j.1365-2141.1995.tb05169.x.
[47] R. Jasuja, B. Furie, B.C. Furie, Endothelium-derived but not platelet-derived protein disulfide isomerase is required for thrombus formation in vivo, Blood 116 (2010) 4665–4674, https://doi.org/10.1182/blood-2010-04-278184.
[48] N. Muller-Calleja, S. Ritter, A. Hollerbach, T. Falter, K.J. Lackner, W. Ruf, Complement C5 but not C3 is expendable for tissue factor activation by cofactor-independent antiphospholipid antibodies, Blood Adv 2 (2018) 979–986, https://doi.org/10.1182/bloodadvances.2018017095.
[49] H. Kobayashi, P.L. Choyke, Target-cancer-cell-specific activatable fluorescence imaging probes: rational design and in vivo applications, Acc. Chem. Res. 44 (2011) 83–90, https://doi.org/10.1021/ar1000633.